Assessing the activity of benzodioxol, phenol and aniline derivatives as radical trapping antioxidants that inhibit ferroptosis

Helene B. E. Schricker,[1,#] Mohamed M. Mouzayek,[1,#] Jonas Wanninger,[2] Hala Zahran,[1] Kyra Lützel,[1] Anna V. Milton,[1] Eikan Mishima,[2] Toshitaka Nakamura,[2] Bettina Proneth,[2] Marcus Conrad,[2] David B. Konrad[1,*]

[1] Department of Pharmacy, Ludwig Maximilian University Munich, 81377 Munich, Germany.

[2] Institute of Metabolism and Cell Death, Molecular Targets and Therapeutics Center, Helmholtz Munich, 85764 Neuherberg, Germany.

Ferroptosis Inhibitors, Radical Trapping Antioxidants, Structure-Activity-Relationship, Medicinal Chemistry

ABSTRACT: A small molecule screen has identified a benzodioxol anilide as a ferroptosis inhibitor. To determine the structure-activity relationship (SAR) of this compound class, we have synthesized a library of 35 derivatives followed by testing their ability to inhibit cell death that was induced via RSL3, an inhibitor of the main ferroptosis regulator glutathione peroxidase 4 (GPX4), in the mouse embryonic fibroblast cell line Pfa-1. Choosing 12 representative structures, rescue experiments were performed following the tamoxifen-induced deletion of GPX4 in Pfa-1 cells to complement the pharmacological induction of ferroptosis with a genetic induction and the experiments were extended to the human epithelial lung adenocarcinoma cell line HCC827. To assess if the compounds act as radical trapping antioxidants (RTAs) that scavenge peroxy radicals which drive lipid peroxidation, a hallmark of ferroptotic cell death, we have used a fluorescence-enabled inhibited autoxidation (Fenix) assay. Mitochondria were identified as the site-of-action using an alkynylated benzodioxol probe together with a copper-catalyzed alkyne-azide cycloaddition (CuAAC)-based Alexa Fluor 488 imaging kit. Our SAR study has yielded insights into the substitution-dependent activity of benzodioxol, aniline and phenol groups as RTAs that inhibit ferroptosis which led to the design of MM-12-Urea as a new broadly applicable chemical probe. Since the investigated functional groups are common motifs in small molecule ligands or natural products, we highlight that it is worth testing their ability to act as RTAs to avoid a potentially compounding factor in their bioactivities.

Introduction:

Ferroptosis is an atypical oxidative form of regulated necrotic cell death that is characterized by the peroxidation of membrane phospholipids which contain polyunsaturated fatty acids.[1] This process is dependent on Fe^{2+} which generates hydroxyl (•OH) and hydroperoxyl (•OOH) radicals from H_2O_2 via a Fenton reaction.[2] If the production of these reactive oxygen species (ROS) exceeds beyond the antioxidant capacity of a cell, accumulated lipid peroxides initiate an autoxidation cascade that results in the rupture of the membrane. In general, enzymes that are involved in H_2O_2 production, the oxidation of phospholipids and/or accumulation of Fe^{2+} in cells contribute to ferroptotic cell death, whereas enzymes that inhibit lipid oxidation, reduce lipid peroxides and/or remove Fe^{2+} protect cells from ferroptosis.[3] A central node of the ferroptotic pathway is GPX4.[4,5] This antioxidant enzyme reduces lipid peroxides to the corresponding alcohols through an interplay between the active-site selenocysteine and the cofactor glutathione (GSH).[6] The induced global deletion of *Gpx4* in mice causes acute renal failure and associated death.[5] Apart from renal failure, ferroptosis has been implicated in a variety of tissue[7] and organ injuries[8–10] as well as neurodegenerative,[11,12] cardiovascular,[13] inflammatory[14] and infectious diseases.[15] A key connection was uncovered between the progression of ischemia reperfusion (IR)-induced-acute organ damage and ferroptotic cell death in the lungs, heart, liver and intestinal tract has been extensively studied and validated in animal models.[5,8,9,13] Remarkably, the pharmacological inhibition of ferroptosis with radical trapping antioxidants (RTAs)[16] protect against synchronizing kidney tubular cell death in both severe IR-induced injury as well as oxalate crystal–induced models of acute kidney injury.[17] These ferroptosis inhibitors have also shown beneficial effects in models for brain injuries and neurodegenerative disorders,[18] such Parkinson's disease,[19] Huntington's disease[7] and hemorrhagic stroke.[20]

Several natural RTAs have been identified as anti-ferroptotic defense mechanisms, such as vitamin E (e.g. α-tocopherol),[21] vitamin K (e.g. MK-4),[22] 7-dehydrocholesterol (7-DHC)[23] and glutathione hydropersulfide (GSSH)[24,25] (**Fig. 1A**). The synthetic ferroptosis inhibitors ferrostatin-1 (Fer-1) as well as liproxstatin-1 (Lip-1) were discovered via high-throughput screenings (**Fig 1B**).[1,5] Structure-activity relationship (SAR) studies

were used to complement and optimize these chemical probes which led to the development of phenothiazine 51 (PTZ-51),[26,27] lipophilic 1,8-tetrahydronaphthyridinols (e.g. C15-THN) and UAMC-3203.[21,28–30]

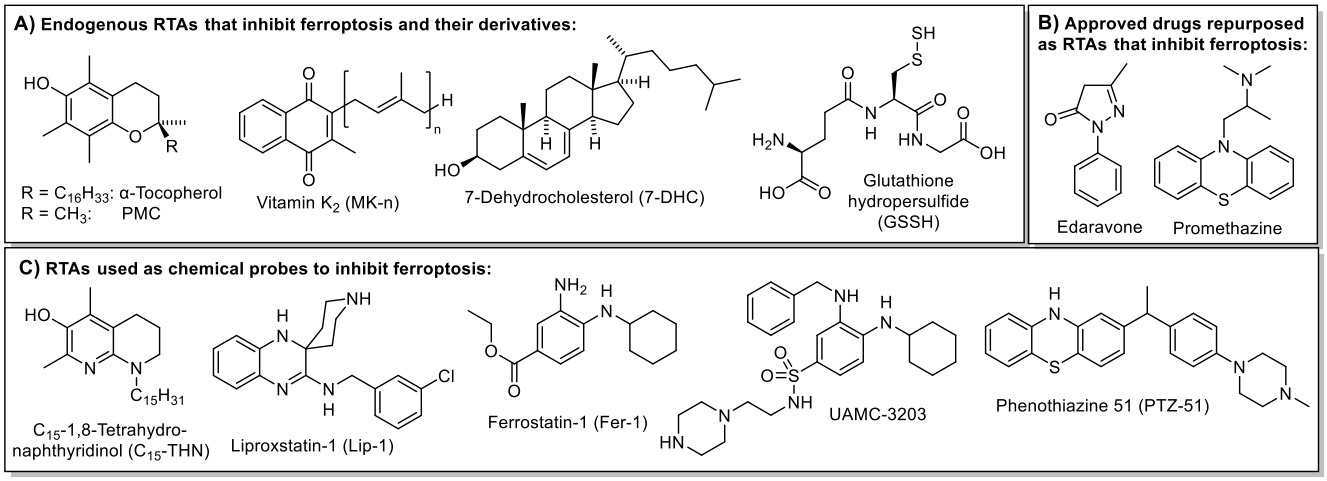

Figure 1. Overview of RTAs that with the ability to inhibit the induction of ferroptosis that were identified in the literature.

While THN derivatives in general constitute potent antioxidants, their ability to rescue cells from ferroptosis required optimizing their interaction with bilayer membranes through appending a lipid side-chain to increase the overall lipophilicity of the molecule.[28] Fer-1 and Lip-1 are predominantly used as chemical tools for studying ferroptosis-related processes in cell-based systems. It was demonstrated that Lip-1 is additionally suitable to *in vivo* studies.[5] While the presence of an electron-withdrawing group was essential for the activity of Fer-1, changing the ester moiety — a functional group well-known to be susceptible to hydrolysis in plasma[7,17,31] — to sulfonamide,[32] significantly improved its ADME properties. A comprehensive medicinal chemistry study on the Fer-1 scaffold yielded UAMC-3203 with a superior potency compared to Fer-1 and a terminal plasma half-life of ~3 h in mice which is suitable to *in vivo* studies.[32,33]

To enable testing the benefits of anti-ferroptotic agents in a clinical setting, approved drugs were studied for their ability to act as RTAs that protected against lipid peroxidation leading to the identification of edaravone[34] and promethazine.[35] Promethazine contains a phenothiazine scaffold which is a well-known RTA that was found to inhibit the induction of ferroptosis alongside phenoxazines and diarylamines.[26,36,37] While these compounds allow to investigate the potential of inhibiting ferroptosis in human subjects suffering from a particular condition, they are not broadly effective or applicable to long-term usage which is required for e.g. neurodegenerative or inflammatory diseases, due to severe side effects and/or off-target binding. Promethazine, for instance, demonstrates activity on a range of receptors that produce its activity as an antihistamine, antipsychotic, sedative, and antiemetic used to treat allergies, insomnia, and nausea with confusion and sleepiness being the most prominent side-effects. Edaravone is used to treat stroke and early-stage amyotrophic lateral sclerosis (ALS). It has shown to be effective in only a narrow ALS patient population and it can cause hypersensitivity reactions as well as common adverse effects such as bruising, gait disturbances, headache, skin inflammation, eczema, problems breathing, excess sugar in urine, and fungal skin infections. As such, the quest for new RTA-based scaffolds with anti-ferroptotic activity is still ongoing to generate insights into SAR profiles and thereby aid the effort to generate drug candidates.

Results:

With the goal to identify cysteine-reactive ferroptosis inhibitors, a library of ~50 structurally diverse acrylamide-substituted small molecules were synthesized in our laboratory. These compounds were employed at a concentration of 25 µM to assesses their ability to rescue a small panel of Non-Small Cell Lung Cancer (NSCLC) cell lines, i.e. HCC827, H1975 and H358, which were sensitive to the inhibition of GPX4 and treated with the ferroptosis inducer RSL3 at its cell-type-specific EC_{90}. Within our small molecule library, KL169 was identified to significantly increase the viability in all the tested cell lines. To investigate whether its activity relied on its reactivity towards cysteine residues, we have synthesized MM-1-1, which harbored a non-reactive propanamide group. Since this compound also had the ability to inhibit RSL3-induced ferroptosis in NSCLC cells, we deduced that the activity of KL169 did not stem from its ability to react with cysteine residues. Due to the small fragment-like size of MM-1-1, we reasoned that it was unlikely to bind to a protein through a non-covalent, reversible mechanism to an extent that it would exert a strong inhibitory action onto its target at a 25 µM concentration.[38] In addition, the similarity of its activity to Fer-1 led to the hypothesis that the compound acts as an RTA. To aid in confirming our hypothesis and since no SAR was established for benzodioxol derivatives complemented by anilide groups as potential anti-ferroptotic RTAs to date, we synthesized a library of 34 derivatives to investigate the following principles: **1)** The impact of the lipid tail length on their ability to inhibit ferroptosis (**Fig 2B**). Studies on the THN scaffold showed that increasing the lipophilicity by appending longer lipid

tails enhanced the ability to interact with bilayer membranes, a requirement to enable the inhibition of ferroptosis.[28] In addition, it was described that a substitution of pharmacophores with medium-size lipids can increase bioactivity and the ability to pass through membranes.[39] **2)** The visualization of the intracellular localization by enabling bioorthogonal CuAAC with between a terminal alkyne groups and fluorophore azides (**Fig 2C**). This investigation will gain insights into the organelle that is involved in the activity of the compounds and are therefore associated with the progression of ferroptosis. **3)** The influence of the stereoelectronic properties of the aromatic functionality on the small molecule activity (**Fig 2D**). **4)** The importance of the amide group for the ability to inhibit ferroptosis (**Fig 2E**). **5)** The ability to increase the antiferropototic activity of a molecule by stitching two aromatic head-groups together using a urea moiety.

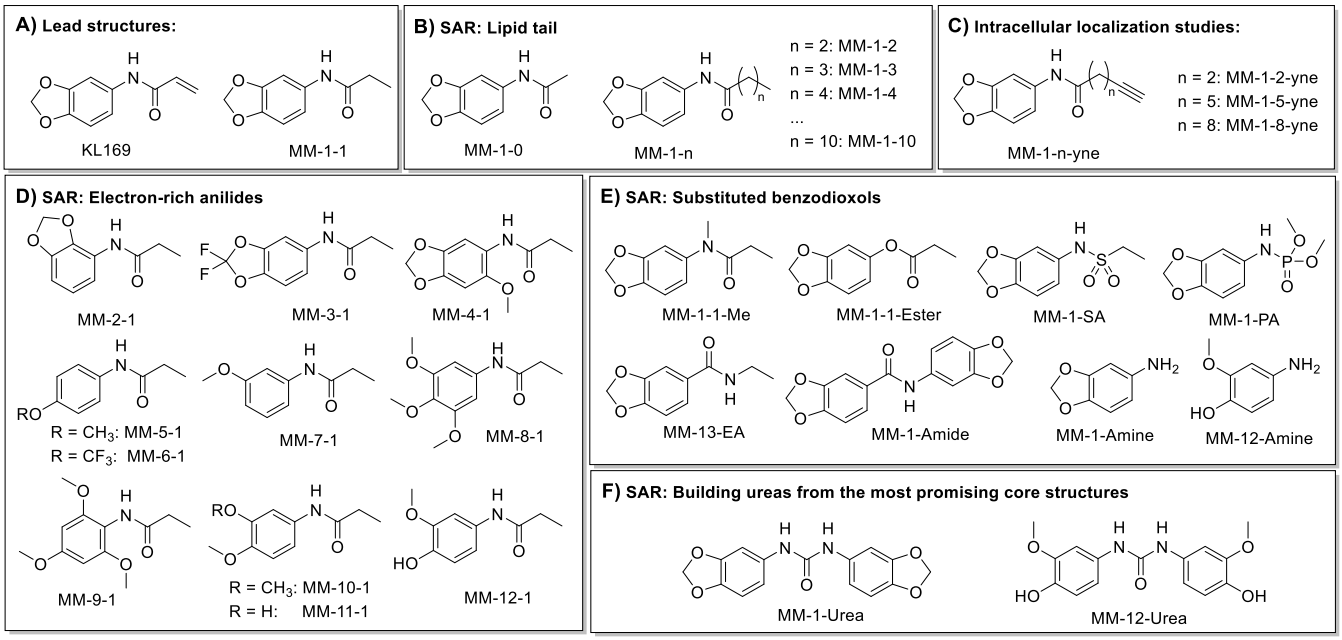

Figure 2. Small molecule library to investigate the SAR profile of the lead structures KL169 and MM-1-1.

Albeit we identified the activity of KL169 and MM-1-1 in NSCLC cell lines, we have performed the initial SAR characterization in the 4-hydroxytamoxifen (TAM)-inducible *Gpx4*$^{-/-}$ mouse embryonic fibroblasts Pfa-1,[12] since they were used in many studies to characterize RTAs with the ability to inhibit ferroptosis. Doing so holds the advantage to enable comparing our results to prior investigations and, while the NSCLC cells can only be used to test the impact of the pharmacological induction of ferroptosis, the Pfa-1 cells additionally allow to assess the impact of the RTAs on the genetic *Gpx4* deletion.[5,21,36]

We first tested the concentration-dependent toxicity of the small molecules through a resazurin viability assay (**Fig. S1A**, Supporting Information p. 27). Lip-1, which was reported to have an EC_{50} value of 22 nM and a TC_{50} value of 6 µM,[5] was included as a reference. MM-12-Amine and Lip-1 were identified to become toxic at concentrations higher than 8.1 µM. MM-12-Urea showed a viability decrease below 25% from 32.5 µM and MM-3-1 from 75 µM. MM-1-6, MM-1-1-Ester and MM-1-Amine became toxic (viability below 25%) at a concentration of 150 µM. At 300 µM, the viability dropped below 25% for MM-6-1. This experiment showed that most compounds did not strongly affect the viability of the Pfa-1 cells. Next, we assessed the concentration-dependent ability of our potential RTA library to rescue Pfa-1 cells after the induction of ferroptosis with 100 nM RSL3 (**Fig. 3A**). The most potent ferroptosis inhibitor, Lip-1, showed a complete rescue at a 1 µM concentration, which is in accordance with its reported EC_{50} value in the low nanomolar range. At 8.1 µM, the benzodioxol amide MM-1-1 and phenol urea MM-12-Urea rescued the Pfa-1 cells by more than 60% and 80%, respectively. Due to the lack of toxicity, the activity of MM-1-1 extended to a concentration of 300 µM, while the viability with MM-12-Urea dropped below 25% again from 32,5 µM. MM-1-1-Ester slightly raised the viability within a concentration range of 8.1 µM and 75 µM to between 25% to 45%. MM-1-Urea showed a concentration dependent increase in cell viability from 16.3 µM to 32.5 µM up to ~60% which was followed by a decrease from 75 µM to 300 µM to ~32%, likely originating from an increasing toxicity of the compound. At 32.5 µM, the benzodioxol amides MM-2-1 and KL169, the phenol amide MM-12-1 as well as the benzodioxol amine MM-1-Amine gained the capacity to rescue Pfa-1 cells (viability >25%) from RSL3-mediated ferroptosis. The viability increase with MM-2-1 and MM-1-Urea was retained up to a concentration of 75 µM before gradually dropping below 20% at 300 µM. For KL169, the viability reached a maximum of ~64% at 150 µM while MM-12-1 fully rescued the cells at 300 µM. Compounds that gained the ability to inhibit ferroptosis at a concentration of 75 µM and beyond included the benzodioxol amides MM-1-3, MM-1-4, MM-1-5-yne, MM-1-SA and MM-1-PA. It is worth noting that, due to a limited solubility from a concentration of 150 µM for MM-1-7, from 75 µM for MM-1-8-yne and from 8.1 µM for MM-1-8, MM-1-9 as well as MM-1-10, the corresponding values were excluded.

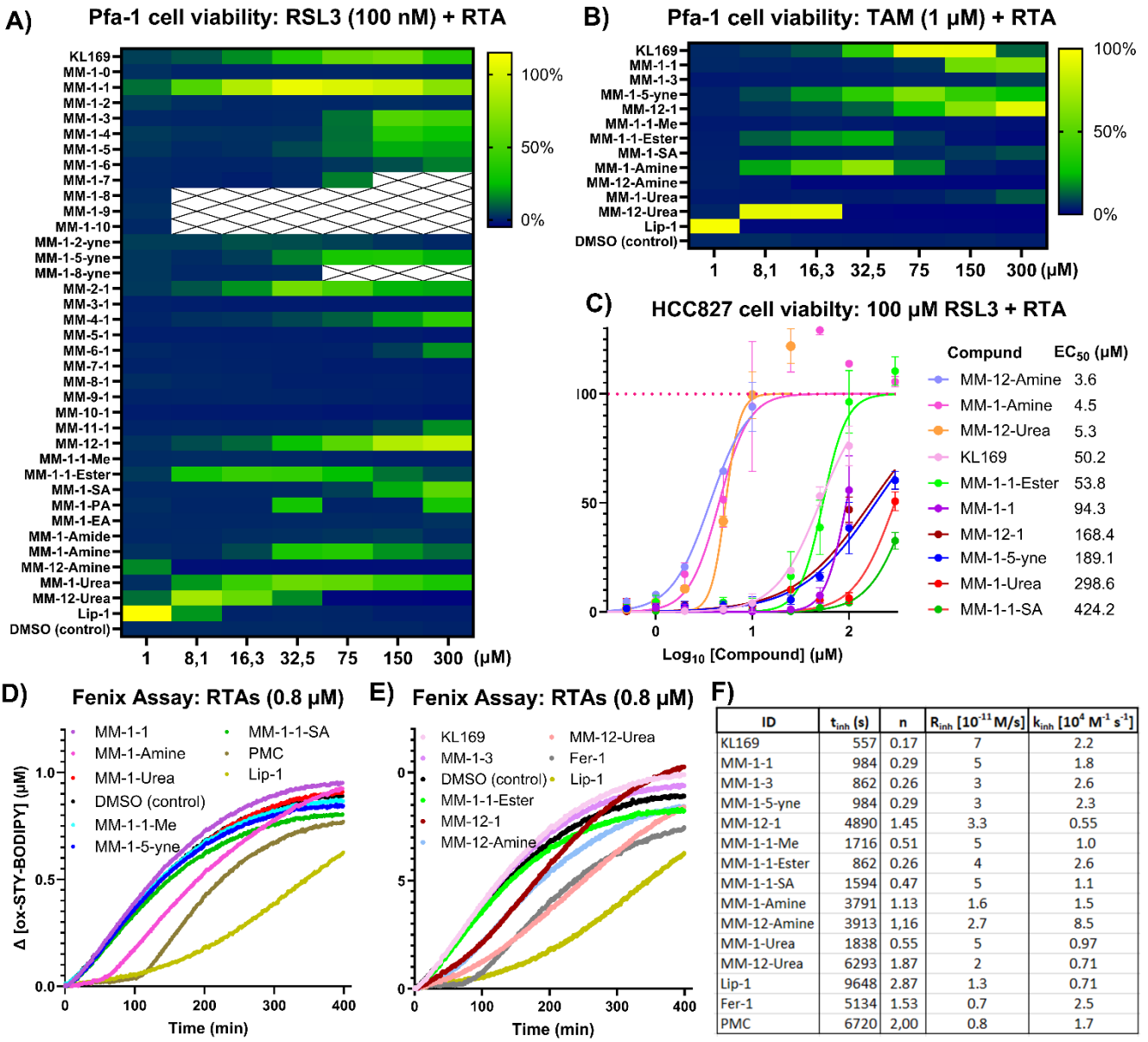

ID	t_{inh} (s)	n	R_{inh} [10^{-11} M/s]	k_{inh} [10^4 M^{-1} s^{-1}]
KL169	557	0.17	7	2.2
MM-1-1	984	0.29	5	1.8
MM-1-3	862	0.26	3	2.6
MM-1-5-yne	984	0.29	3	2.3
MM-12-1	4890	1.45	3.3	0.55
MM-1-1-Me	1716	0.51	5	1.0
MM-1-1-Ester	862	0.26	4	2.6
MM-1-1-SA	1594	0.47	5	1.1
MM-1-Amine	3791	1.13	1.6	1.5
MM-12-Amine	3913	1,16	2.7	8.5
MM-1-Urea	1838	0.55	5	0.97
MM-12-Urea	6293	1.87	2	0.71
Lip-1	9648	2.87	1.3	0.71
Fer-1	5134	1.53	0.7	2.5
PMC	6720	2,00	0.8	1.7

Figure 3. Assessing the ability of the potential RTAs to rescue Pfa-1 (**A**) and HCC827 (**C**) cells from the pharmacological induction of ferroptosis using RSL3. **B)** Rescue experiments following the induction of ferroptosis through the genetic deletion of GPX4 induced by TAM treatment. **D)** and **E)** Visualization of the compound- and time-dependent increase in oxidated STY-BODIPY in a Fenix assay. **F)** Values for the duration of inhibition, stoichiometry for the trapping of peroxyl radicals, rate of inhibition and inhibition rate constants.

From this point, we selected 12 molecules out of our library which were used to perform a detailed investigation into their activity. Our selection included 11 structurally diverse ferroptosis inhibitors with different activity levels along with MM-1-1-Me as a negative control. To complement the rescue experiments that were performed with the RTAs in response to the pharmacological induction of ferroptosis with RSL3, we have assessed the activity of the compounds in concert with the TAM-induced genetic deletion of *Gpx4* (**Fig. 3B**). This approach enables to exclude the possibility that the evaluated chemical probes act e.g. through by interfering with the action of RSL3 or by engaging with GPX4. The results showed similar activities and overall trends, with two exceptions: MM-1-Urea and MM-12-Amine did not demonstrate the ability to rescue Pfa-1 cells at the concentrations that were tested, and MM-1-1 has a significantly decreased activity. Next, we assessed if the compounds have a general activity as ferroptosis inhibitors by expanding the tests to the human epithelial lung adenocarcinoma cell line HCC827. To identify optimal conditions that would allow us to evaluate the effects of RTAs in this cell line, we studied the concentration- and duration-dependent effects of RSL3 on cell viability complemented by rescue experiments with Fer-1 (2 μM). These experiments allowed us to generate dose-response curves for 24, 48 and 72 h treatment periods (**Fig. S1C-D**, Supporting Information p. 27). The biggest impact of Fer-1 on cell viability was found after 24 h where the EC_{50} was

shifted by a factor of ~200 from 36 nM to 6.5 µM through the addition of Fer-1. In this setting, inducing ferroptosis with 100 nM RSL3 which roughly corresponds to the EC_{90} value could still be fully rescued and thereby constitutes and ideal experimental set-up for testing our compounds. In these tests, we set out to determined EC_{50} values for each studied example (**Fig. 3C**). We found that the three most potent ferroptosis inhibitors MM-12-Amine, MM-1-Amine and MM-12-Urea harbored EC_{50} values of 3.6, 4.5 and 5.3 µM, respectively. Intriguingly, the viability that was observed through rescue experiments with MM-12-Urea (≥10 µM, <50 µM) and MM-1-Amine (≥10 µM) in the resazurin assay was higher than that of the vehicle-treated cells. The originally identified compounds KL169 (EC_{50} = 50.2 µM) and MM-1-1 (EC_{50} = 94.3 µM) along with MM-1-1-Ester (EC_{50} = 53.8 µM), produced a moderate effect. MM-12-1 (EC_{50} = 168.4 µM), MM-1-5-yne (EC_{50} = 189.1 µM), MM-1-Urea (EC_{50} = 298.6 µM) and MM-1-1-SA (EC_{50} = 424.2 µM) were active but had a low potency. For the compounds MM-1-1-Me and MM-1-3, no activity was observed in a concentration range up to 300 µM. Analogous to the experiments in Pfa-1 cells, we found that Lip-1 MM-12-Amine as well as MM-12-Urea became toxic at elevated concentrations, whereby the corresponding TC_{50} values were 8.1, 25.9 and 98.9 µM, respectively (**Fig. S1E**, Supporting Information p. 27).

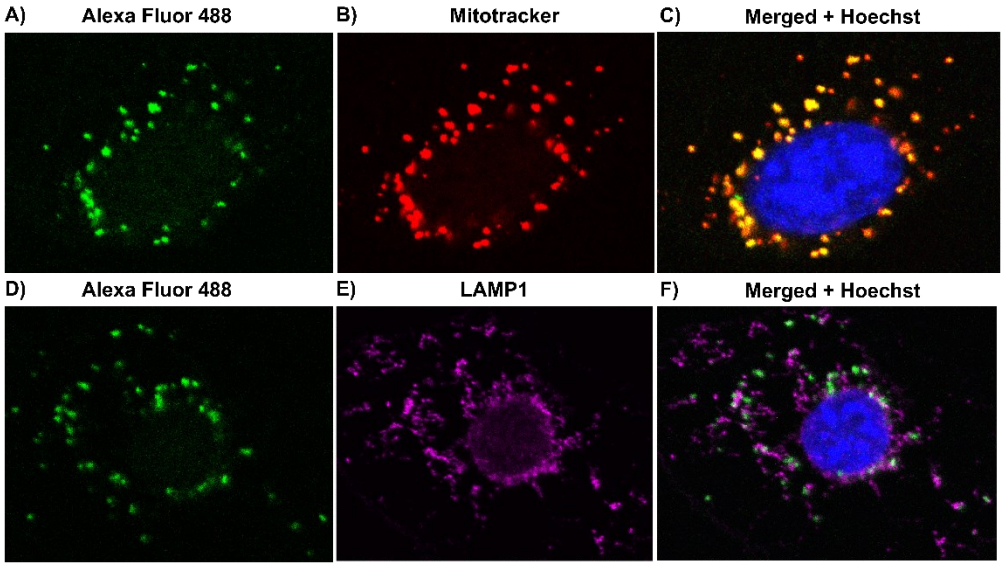

Figure 4. Determining the subcellular compartment that serves as the RTA site-of-action. **A)** and **D)** MM-1-5-yne coupled *in situ* to Alexa Fluor 488 in green. **B)** Mitochondrial staining using Mitotracker in red. **C)** Merging **A** and **B** together with nuclear staining using the Hoechst dye in blue. **E)** Lysosomal staining with the LAMP1 antibody. **F)** Merging **D** and **E** together with nuclear staining using the Hoechst dye in blue.

To assess whether the effects of the compounds stem from their ability to act as an RTAs, we performed a fluorescence-enabled inhibited autoxidation (Fenix) assay.[21,40] A Fenix assay allows to investigate the reactivity of small molecules towards peroxyl radicals in the lipid bilayers of unilamellar liposomes prepared from egg phosphatidylcholine (PC). The reaction progress is monitored through the competitive oxidation of the fluorescent substrate STY-BODIPY (**Fig. 3D** and **E**). To enable relating our results to those available in the literature, we included Lip-1, Fer-1 and PMC as benchmarks together with the 12 compounds that were selected from our library. The experiments were performed using a 0.81 µM concentration for each small molecule. In accordance with prior results,[21] we found that Fer-1 and PMC have similar reactivities with rate constants of $k_{inh} = 2.5 \times 10^4\ M^{-1}s^{-1}$ and $k_{inh} = 1.7 \times 10^4\ M^{-1}s^{-1}$, respectively (**Fig. 3F**). Compared to Fer-1, the reactivity of Lip-1 is decreased by a factor of ~3.5 to $k_{inh} = 0.7 \times 10^4\ M^{-1}s^{-1}$. We observed reactivities similar to Fer-1 and PMC with the benzodioxol-derived KL169, MM-1-1, MM-1-3, MM-1-5-yne and MM-1-1-Ester with $k_{inh} \geq 1.8 \times 10^4\ M^{-1}s^{-1}$. The aminophenol MM-12-Amine has a particularly high reactivity with $k_{inh} = 8.5 \times 10^4\ M^{-1}s^{-1}$. Medium level reactivities ($1.7 \times 10^4\ M^{-1}s^{-1} \geq k_{inh} \geq 1.0 \times 10^4\ M^{-1}s^{-1}$) were found for MM-1-1-SA, MM-1-1-Me and MM-1-Amine. Low reactivities ($k_{inh} < 1.0 \times 10^4\ M^{-1}s^{-1}$) were determined for MM-12-1, MM-1-Urea and MM-12-Urea. The stoichiometry for the trapping of peroxyl radicals was normalized to the inhibited periods for PMC, which is a well-studied RTA in the literature with n = 2.[21] The benzodioxol-derived KL169, MM-1-1, MM-1-3, MM-1-5-yne, MM-1-1-Me, MM-1-1-Ester, MM-1-1-SA and MM-1-Urea had low stoichiometries (n < 1). MM-12-1, MM-1-Amine, MM-12-Amine and MM-12-Urea had a comparable ability to trap peroxyl radicals to Fer-1 with 1 ≤ n < 2. Only Lip-1 showed a stoichiometry higher than 2.

Finally, we set out to identify the subcellular compartment that serves as the site-of-action for the newly discovered class of RTAs with the Click-iT Alexa Fluor 488 Imaging Kit in combination with confocal microscopy. Pfa-1 cells were treated with the alkynylated MM-1-5-yne as a representative structure at a concentration (150 µM) close to its EC_{50} value as a ferroptosis inhibitor. After fixing the cells, an intracellular CuAAC was performed with an azide-substituted Alexa Fluor™ 488 dye to visualize the localization of the RTA (**Fig. 4A** and **D**). This was complemented by a staining with MitoTracker™ Red CMXRos dye to highlight the mitochondria (**Fig. 4B**) or the LAMP1 antibody to highlight lysosomes (**Fig. 4E**). Merging **Fig. 4A** and **B** with nuclear staining using the Hoechst dye (**Fig. 4C**) confirmed accumulation in mitochondria as potential site-of-action, while merging **Fig. 4D** and **E** ruled out lysosomal localization.

Discussion:

The bond dissociation energy (BDE) for a homolytic hydrogen abstraction from the benzodioxol methylene group is 374 kJ/mol[41] while the anilide N-H bond corresponds to414 kJ/mol.[42] As such, we reason that the functional group that imparts KL169, MM-1-1, MM-1-3, MM-1-4, MM-1-5-yne, MM-2-1 and MM-1-Urea with the ability to inhibit ferroptosis is the benzodioxol moiety. This hypothesis is supported by the finding that substituting the benzodioxol hydrogen atoms on MM-1-1 with fluorine or changing the substitution pattern on the aryl group (MM-5-1 – MM-11-1, **Fig. 2D**) abolishes the activity in Pfa-1 cells. Retaining a benzodioxol substitution but shifting the arrangement of the functionalities or adding additional substituents (MM-2-1 and MM-4-1, respectively) that change the orientation or flexibility of the amide group, which can act as both hydrogen bond donor and acceptor, retains the ability to inhibit cell death, but decreases the potency. Prior studies have shown that hydrogen bonding between RTAs and the phosphatidylcholine head group influences the activity RTAs in lipid bilayers.[26] As such, we are considering that the amide group functions as a hydrogen bond donor which can contribute to the arrangement of the compounds within the membrane and thereby increase their potency as RTAs. Modulating the length of the lipid chain (MM-1-0, MM-1-2, MM-1-5 – MM-1-10, MM-1-2-yne and MM-1-8-yne, **Fig. 2B** and **C**), in this regard, likely abolishes the biological activity by an unfavorable arrangement of the hydrogen radical donor within the lipid bilayer or by leading to a decreased solubility in aqueous media. As part of our assessment of different aryl structures, we have found that substituting the benzodioxol with a methoxyphenol group (MM-12-1) led to an active ferroptosis inhibitor at concentrations >32.5 μM. Derivatives of phenol, which has a BDE of 365 kJ/mol,[43] such as α-tocopherol and 2,2,5,7,8-pentamethyl-6-chromanol (PMC, **Fig. 1A**) were described in the literature as RTAs.[21,40] Exchanging the arrangement of the methoxy and hydroxy groups to position the OH functionality *meta* to the amide (MM-11-1), however, abolished the activity. We reason that this finding results from a combination of two factors: 1) Moving the electron-donating propylamide substituent from the *para* to the *meta* position decreases its ability to stabilize a phenoxy radical; and 2) The positioning of the compound within a lipid bilayer is modified due to a potential hydrogen bonding interaction between the amide proton and the phosphate group on PC. Next, we performed a more detailed investigation into the connection between the activity and the properties of the hydrogen bonding donor (**Fig. 2E**) using benzodioxol (MM-1-1) as a lead structure. Removing the hydrogen-bond donor (MM-1-1-Me), moving from an anilide to a benzamide structure that either hosts an ethyl (MM-13-EA) or a second benzodioxol (MM-1-Amide) substituent removes the ability to inhibit ferroptosis, likely owning to a poor supramolecular arrangement of the compounds within a membrane. Modulating the strength of the hydrogen bond donor by using a sulfonamide (MM-1-SA) or phosphate amide (MM-1-PA) weakens the activity but retains the ability to inhibit ferroptosis at high concentrations. Intriguingly, formally exchanging the amine group with oxygen to generate an ester (MM-1-1-Ester) demonstrates a moderate rescue activity at concentrations between 8.1 – 75 μM. It is well-known that ester groups are susceptible to hydrolysis in plasma.[17,31] As such, it is reasonable to assume that the activity of MM-1-1-Ester stems from the formation of the corresponding phenol with the cell. Even though aniline has a high BDE of 387 kJ/mol,[44] the active motif within Fer-1 and Lip-1 are aromatic amine groups. This is why we have next complemented the benzodioxol and phenol groups with an aniline structure by formally cleaving the propylamide within MM-1-1 and MM-12-1 to give MM-1-Amine and MM-12-Amine. In the Pfa-1 cells, MM-1-Amine was moderately active as a ferroptosis inhibitor with a low toxicity, while MM-12-Amine demonstrated an activity below an 8.1 μM concentration and became toxic at concentrations above 8.1 μM. Since anilines tend to be slowly oxidized by air[45] which limits their utility due to an inability to store these compounds for prolonged periods of time without decomposition, we aimed to identify a derivative that has a similar activity and remains stable. Based on our findings, we hypothesized that employing a urea moiety is a promising choice since it hosts a similar BDE (389 kJ/mol)[46] as aniline, can function as a hydrogen bond donor and, at the same time, link two benzodioxol (MM-1-Urea) or methoxyphenol groups (MM-12-Urea) together to double the number of hydrogen radical donors per molecule. While MM-1-Urea had a low activity, MM-12-Urea exhibited a high activity at an 8.1 and 16.3 μM concentration with a toxicity that emerged at 32.5 μM.

We found that KL169, MM-1-1-Me, MM-12-Urea and Lip-1 have similar activities between the two conditions used with Pfa-1 cells and one condition used with HCC827. However, the level of activity of MM-1-1, MM-1-3, MM-1-5-yne, MM-1-1-Ester, MM-1-1-SA, MM-12-1, MM-1-Amine and MM-12-Amine showed a dependency on the conditions and the cell lines that were used. By correlating our results in the HCC827 viability assays with the Fenix assay, we found that compounds with a high stoichiometry for the trapping of peroxyl radicals are, in many cases, better ferroptosis inhibitors. Examples for this observation are MM-1-Amine, MM-12-Amine and MM-12-Urea. MM-12-1 with n = 1.45, however, showed only a moderate activity. Apart from the amine-substituted variant, the benzodioxol scaffold hosted low stoichiometries (n < 0.6), while the derivatives that displayed higher activities in the inhibition of ferroptosis were found to harbor higher reactivities (k_{inh} > 1.8×10^4 $M^{-1}s^{-1}$). Based on its ability to produce analogous effects between the cell lines and conditions that were used, along with one of the highest potencies that were observed in this study, we reason that MM-12-Urea is the most promising RTA-based chemical probe amongst the investigated compound library to inhibit the induction of ferroptosis.

Conclusion:

Our results suggest that benzodioxols are moderate radical trapping antioxidants whereby their activity is subject to strong shifts based on slight variations of the substitution pattern. Albeit potent RTAs commonly contain phenol or aniline groups, we found that the potency of chemical probes that host these functionalities strongly depends on the nature and relative positioning of the substituents that are installed on the same aryl group. For example, the phenol derivatives MM-11-1 and MM-12-1 have low to moderate activities, while MM-12-Urea and MM-12-Amine are highly active. We reason that these effects stem from two factors: 1) The ability to stabilize a phenoxy radical; and 2) The propensity to favorably position the compound within a lipid bilayer through potential hydrogen bonding interaction with the phosphate group on PC. Based on these factors, the benzodioxol group can produce a stronger effect as RTA-based ferroptosis inhibitor than phenol derivatives by embedding the functionality into an ideal scaffold. This tend becomes apparent when comparing the benzodioxol-derived KL169 with the phenol-derived MM-11-1 and MM-12-1.

In conclusion, our SAR study has yielded insights into the substitution-dependent activity of benzodioxol, phenol and aniline as RTAs that inhibit ferroptosis which led to the design of MM-12-Urea as a new broadly applicable chemical probe. By employing the Click-iT Alexa Fluor 488 Imaging Kit, we showed that the site-of-action of benzodioxol-derived MM-1-5-yne are the mitochondria. This finding provides an association between the progression of ferroptotic cell death and mitochondria since blocking lipid peroxidation in this organelle inhibits the induction of cell death. Since phenol,[47] aniline[48] or benzodioxol[49] functional groups are common motifs in small molecule ligands or natural products, it is worth cautioning that their ability to act as RTAs, if undesired, can potentially pose a compounding factor in their bioactivities.

AUTHOR INFORMATION

Corresponding Author

* David B. Konrad – Department of Pharmacy, Ludwig Maximilian University Munich, 81377 Munich, Germany; orcid.org/0000-0001-5718-8081, Phone: +49 89 2180 77273, Email: david.konrad@cup.lmu.de

Author Contributions

# HBES and MMM contributed equally.

ACKNOWLEDGMENT

DBK is grateful to the Fonds der chemischen Industrie for a Liebig fellowship. This work was supported by the Deutsche Forschungsgemeinschaft (DFG) (CO 291/7-1 to MC and PR 1752/3-1 to BP) and the Priority Program SPP 2306 (CO 291/9-1, no. 461385412 and CO 291/10-1, no. 461507177 to MC and KO 5903/2-1, no. 461576077 to DBK), the German Federal Ministry of Education and Research (BMBF) FERROPATH (01EJ2205B), and the European Research Council (ERC) under the European Union's Horizon 2020 research and innovation program (grant agreement no. GA 884754) to M.C. AVM ackowledges the Studienstiftung des deutschen Volkes and the Marianne-Plehn-Program for scholarships. The authors thank Luke A Farmer and Derek A. Pratt for advice on the Fenix assay.

REFERENCES

(1) Dixon, S. J.; Lemberg, K. M.; Lamprecht, M. R.; Skouta, R.; Zaitsev, E. M.; Gleason, C. E.; Patel, D. N.; Bauer, A. J.; Cantley, A. M.; Yang, W. S.; Morrison, B.; Stockwell, B. R. Ferroptosis: An Iron-Dependent Form of Nonapoptotic Cell Death. *Cell* **2012**, *149* (5), 1060–1072. https://doi.org/10.1016/j.cell.2012.03.042.

(2) Dixon, S. J.; Stockwell, B. R. The Role of Iron and Reactive Oxygen Species in Cell Death. *Nat Chem Biol* **2014**, *10* (1), 9–17. https://doi.org/10.1038/nchembio.1416.

(3) Milton, A. V.; Konrad, D. B. Epithelial-Mesenchymal Transition and H_2O_2 Signaling – a Driver of Disease Progression and a Vulnerability in Cancers. *Biological Chemistry* **2022**, *403* (4), 377–390. https://doi.org/10.1515/hsz-2021-0341.

(4) Yang, W. S.; SriRamaratnam, R.; Welsch, M. E.; Shimada, K.; Skouta, R.; Viswanathan, V. S.; Cheah, J. H.; Clemons, P. A.; Shamji, A. F.; Clish, C. B.; Brown, L. M.; Girotti, A. W.; Cornish, V. W.; Schreiber, S. L.; Stockwell, B. R. Regulation of Ferroptotic Cancer Cell Death by GPX4. *Cell* **2014**, *156* (1), 317–331. https://doi.org/10.1016/j.cell.2013.12.010.

(5) Friedmann Angeli, J. P.; Schneider, M.; Proneth, B.; Tyurina, Y. Y.; Tyurin, V. A.; Hammond, V. J.; Herbach, N.; Aichler, M.; Walch, A.; Eggenhofer, E.; Basavarajappa, D.; Rådmark, O.; Kobayashi, S.; Seibt, T.; Beck, H.; Neff, F.; Esposito, I.; Wanke, R.; Förster, H.; Yefremova, O.; Heinrichmeyer, M.; Bornkamm, G. W.; Geissler, E. K.; Thomas, S. B.; Stockwell, B. R.; O'Donnell, V. B.; Kagan, V. E.; Schick, J. A.; Conrad, M. Inactivation of the Ferroptosis Regulator Gpx4 Triggers Acute Renal Failure in Mice. *Nat Cell Biol* **2014**, *16* (12), 1180–1191. https://doi.org/10.1038/ncb3064.

(6) Thomas, J. P.; Geiger, P. G.; Maiorino, M.; Ursini, F.; Girotti, A. W. Enzymatic Reduction of Phospholipid and Cholesterol Hydroperoxides in Artificial Bilayers and Lipoproteins. *Biochimica et Biophysica Acta (BBA) - Lipids and Lipid Metabolism* **1990**, *1045* (3), 252–260. https://doi.org/10.1016/0005-2760(90)90128-K.

(7) Skouta, R.; Dixon, S. J.; Wang, J.; Dunn, D. E.; Orman, M.; Shimada, K.; Rosenberg, P. A.; Lo, D. C.; Weinberg, J. M.; Linkermann, A.; Stockwell, B. R. Ferrostatins Inhibit Oxidative Lipid Damage and Cell Death in Diverse Disease Models. *J. Am. Chem. Soc.* **2014**, *136* (12), 4551–4556. https://doi.org/10.1021/ja411006a.

(8) Li, Y.; Feng, D.; Wang, Z.; Zhao, Y.; Sun, R.; Tian, D.; Liu, D.; Zhang, F.; Ning, S.; Yao, J.; Tian, X. Ischemia-Induced ACSL4 Activation Contributes to Ferroptosis-Mediated Tissue Injury in Intestinal Ischemia/Reperfusion. *Cell Death Differ* **2019**, *26* (11), 2284–2299. https://doi.org/10.1038/s41418-019-0299-4.

(9) Li, Y.; Cao, Y.; Xiao, J.; Shang, J.; Tan, Q.; Ping, F.; Huang, W.; Wu, F.; Zhang, H.; Zhang, X. Inhibitor of Apoptosis-Stimulating Protein of P53 Inhibits Ferroptosis and Alleviates Intestinal Ischemia/Reperfusion-Induced Acute Lung Injury. *Cell Death Differ* **2020**, *27* (9), 2635–2650. https://doi.org/10.1038/s41418-020-0528-x.

(10) Jiang, X.; Stockwell, B. R.; Conrad, M. Ferroptosis: Mechanisms, Biology and Role in Disease. *Nat Rev Mol Cell Biol* **2021**, *22* (4), 266–282. https://doi.org/10.1038/s41580-020-00324-8.

(11) Hambright, W. S.; Fonseca, R. S.; Chen, L.; Na, R.; Ran, Q. Ablation of Ferroptosis Regulator Glutathione Peroxidase 4

in Forebrain Neurons Promotes Cognitive Impairment and Neurodegeneration. *Redox Biology* **2017**, *12*, 8–17. https://doi.org/10.1016/j.redox.2017.01.021.

(12) Seiler, A.; Schneider, M.; Förster, H.; Roth, S.; Wirth, E. K.; Culmsee, C.; Plesnila, N.; Kremmer, E.; Rådmark, O.; Wurst, W.; Bornkamm, G. W.; Schweizer, U.; Conrad, M. Glutathione Peroxidase 4 Senses and Translates Oxidative Stress into 12/15-Lipoxygenase Dependent- and AIF-Mediated Cell Death. *Cell Metabolism* **2008**, *8* (3), 237–248. https://doi.org/10.1016/j.cmet.2008.07.005.

(13) Fang, X.; Wang, H.; Han, D.; Xie, E.; Yang, X.; Wei, J.; Gu, S.; Gao, F.; Zhu, N.; Yin, X.; Cheng, Q.; Zhang, P.; Dai, W.; Chen, J.; Yang, F.; Yang, H.-T.; Linkermann, A.; Gu, W.; Min, J.; Wang, F. Ferroptosis as a Target for Protection against Cardiomyopathy. *Proc. Natl. Acad. Sci. U.S.A.* **2019**, *116* (7), 2672–2680. https://doi.org/10.1073/pnas.1821022116.

(14) Li, P.; Jiang, M.; Li, K.; Li, H.; Zhou, Y.; Xiao, X.; Xu, Y.; Krishfield, S.; Lipsky, P. E.; Tsokos, G. C.; Zhang, X. Glutathione Peroxidase 4–Regulated Neutrophil Ferroptosis Induces Systemic Autoimmunity. *Nat Immunol* **2021**, *22* (9), 1107–1117. https://doi.org/10.1038/s41590-021-00993-3.

(15) Xu, S.; Min, J.; Wang, F. Ferroptosis: An Emerging Player in Immune Cells. *Science Bulletin* **2021**, *66* (22), 2257–2260. https://doi.org/10.1016/j.scib.2021.02.026.

(16) Scarpellini, C.; Klejborowska, G.; Lanthier, C.; Hassannia, B.; Vanden Berghe, T.; Augustyns, K. Beyond Ferrostatin-1: A Comprehensive Review of Ferroptosis Inhibitors. *Trends in Pharmacological Sciences* **2023**, *44* (12), 902–916. https://doi.org/10.1016/j.tips.2023.08.012.

(17) Linkermann, A.; Skouta, R.; Himmerkus, N.; Mulay, S. R.; Dewitz, C.; De Zen, F.; Prokai, A.; Zuchtriegel, G.; Krombach, F.; Welz, P.-S.; Weinlich, R.; Vanden Berghe, T.; Vandenabeele, P.; Pasparakis, M.; Bleich, M.; Weinberg, J. M.; Reichel, C. A.; Bräsen, J. H.; Kunzendorf, U.; Anders, H.-J.; Stockwell, B. R.; Green, D. R.; Krautwald, S. Synchronized Renal Tubular Cell Death Involves Ferroptosis. *Proc. Natl. Acad. Sci. U.S.A.* **2014**, *111* (47), 16836–16841. https://doi.org/10.1073/pnas.1415518111.

(18) Tuo, Q.; Lei, P.; Jackman, K. A.; Li, X.; Xiong, H.; Li, X.; Liuyang, Z.; Roisman, L.; Zhang, S.; Ayton, S.; Wang, Q.; Crouch, P. J.; Ganio, K.; Wang, X.; Pei, L.; Adlard, P. A.; Lu, Y.; Cappai, R.; Wang, J.; Liu, R.; Bush, A. I. Tau-Mediated Iron Export Prevents Ferroptotic Damage after Ischemic Stroke. *Mol Psychiatry* **2017**, *22* (11), 1520–1530. https://doi.org/10.1038/mp.2017.171.

(19) Guiney, S. J.; Adlard, P. A.; Bush, A. I.; Finkelstein, D. I.; Ayton, S. Ferroptosis and Cell Death Mechanisms in Parkinson's Disease. *Neurochemistry International* **2017**, *104*, 34–48. https://doi.org/10.1016/j.neuint.2017.01.004.

(20) Zille, M.; Karuppagounder, S. S.; Chen, Y.; Gough, P. J.; Bertin, J.; Finger, J.; Milner, T. A.; Jonas, E. A.; Ratan, R. R. Neuronal Death After Hemorrhagic Stroke In Vitro and In Vivo Shares Features of Ferroptosis and Necroptosis. *Stroke* **2017**, *48* (4), 1033–1043. https://doi.org/10.1161/STROKEAHA.116.015609.

(21) Zilka, O.; Shah, R.; Li, B.; Friedmann Angeli, J. P.; Griesser, M.; Conrad, M.; Pratt, D. A. On the Mechanism of Cytoprotection by Ferrostatin-1 and Liproxstatin-1 and the Role of Lipid Peroxidation in Ferroptotic Cell Death. *ACS Cent. Sci.* **2017**, *3* (3), 232–243. https://doi.org/10.1021/acscentsci.7b00028.

(22) Mishima, E.; Ito, J.; Wu, Z.; Nakamura, T.; Wahida, A.; Doll, S.; Tonnus, W.; Nepachalovich, P.; Eggenhofer, E.; Aldrovandi, M.; Henkelmann, B.; Yamada, K.; Wanninger, J.; Zilka, O.; Sato, E.; Feederle, R.; Hass, D.; Maida, A.; Mourão, A. S. D.; Linkermann, A.; Geissler, E. K.; Nakagawa, K.; Abe, T.; Fedorova, M.; Proneth, B.; Pratt, D. A.; Conrad, M. A Non-Canonical Vitamin K Cycle Is a Potent Ferroptosis Suppressor. *Nature* **2022**, *608* (7924), 778–783. https://doi.org/10.1038/s41586-022-05022-3.

(23) Freitas, F. P.; Alborzinia, H.; Dos Santos, A. F.; Nepachalovich, P.; Pedrera, L.; Zilka, O.; Inague, A.; Klein, C.; Aroua, N.; Kaushal, K.; Kast, B.; Lorenz, S. M.; Kunz, V.; Nehring, H.; Xavier Da Silva, T. N.; Chen, Z.; Atici, S.; Doll, S. G.; Schaefer, E. L.; Ekpo, I.; Schmitz, W.; Horling, A.; Imming, P.; Miyamoto, S.; Wehman, A. M.; Genaro-Mattos, T. C.; Mirnics, K.; Kumar, L.; Klein-Seetharaman, J.; Meierjohann, S.; Weigand, I.; Kroiss, M.; Bornkamm, G. W.; Gomes, F.; Netto, L. E. S.; Sathian, M. B.; Konrad, D. B.; Covey, D. F.; Michalke, B.; Bommert, K.; Bargou, R. C.; Garcia-Saez, A.; Pratt, D. A.; Fedorova, M.; Trumpp, A.; Conrad, M.; Friedmann Angeli, J. P. 7-Dehydrocholesterol Is an Endogenous Suppressor of Ferroptosis. *Nature* **2024**, *626* (7998), 401–410. https://doi.org/10.1038/s41586-023-06878-9.

(24) Barayeu, U.; Schilling, D.; Eid, M.; Xavier Da Silva, T. N.; Schlicker, L.; Mitreska, N.; Zapp, C.; Gräter, F.; Miller, A. K.; Kappl, R.; Schulze, A.; Friedmann Angeli, J. P.; Dick, T. P. Hydropersulfides Inhibit Lipid Peroxidation and Ferroptosis by Scavenging Radicals. *Nat Chem Biol* **2023**, *19* (1), 28–37. https://doi.org/10.1038/s41589-022-01145-w.

(25) Wu, Z.; Khodade, V. S.; Chauvin, J.-P. R.; Rodriguez, D.; Toscano, J. P.; Pratt, D. A. Hydropersulfides Inhibit Lipid Peroxidation and Protect Cells from Ferroptosis. *J. Am. Chem. Soc.* **2022**, *144* (34), 15825–15837. https://doi.org/10.1021/jacs.2c06804.

(26) Farmer, L. A.; Wu, Z.; Poon, J.-F.; Zilka, O.; Lorenz, S. M.; Huehn, S.; Proneth, B.; Conrad, M.; Pratt, D. A. Intrinsic and Extrinsic Limitations to the Design and Optimization of Inhibitors of Lipid Peroxidation and Associated Cell Death. *J. Am. Chem. Soc.* **2022**, *144* (32), 14706–14721. https://doi.org/10.1021/jacs.2c05252.

(27) Yang, W.; Liu, X.; Song, C.; Ji, S.; Yang, J.; Liu, Y.; You, J.; Zhang, J.; Huang, S.; Cheng, W.; Shao, Z.; Li, L.; Yang, S. Structure-Activity Relationship Studies of Phenothiazine Derivatives as a New Class of Ferroptosis Inhibitors Together with the Therapeutic Effect in an Ischemic Stroke Model. *European Journal of Medicinal Chemistry* **2021**, *209*, 112842. https://doi.org/10.1016/j.ejmech.2020.112842.

(28) Li, B.; Harjani, J. R.; Cormier, N. S.; Madarati, H.; Atkinson, J.; Cosa, G.; Pratt, D. A. Besting Vitamin E: Sidechain Substitution Is Key to the Reactivity of Naphthyridinol Antioxidants in Lipid Bilayers. *J. Am. Chem. Soc.* **2013**, *135* (4), 1394–1405. https://doi.org/10.1021/ja309153x.

(29) Wijtmans, M.; Pratt, D. A.; Valgimigli, L.; DiLabio, G. A.; Pedulli, G. F.; Porter, N. A. 6-Amino-3-Pyridinols: Towards Diffusion-Controlled Chain-Breaking Antioxidants. *Angew Chem Int Ed* **2003**, *42* (36), 4370–4373. https://doi.org/10.1002/anie.200351881.

(30) Devisscher, L.; Van Coillie, S.; Hofmans, S.; Van Rompaey, D.; Goossens, K.; Meul, E.; Maes, L.; De Winter, H.; Van Der Veken, P.; Vandenabeele, P.; Berghe, T. V.; Augustyns, K. Discovery of Novel, Drug-Like Ferroptosis Inhibitors with in Vivo Efficacy. *J. Med. Chem.* **2018**, *61* (22), 10126–10140. https://doi.org/10.1021/acs.jmedchem.8b01299.

(31) Di, L.; Kerns, E. H.; Hong, Y.; Chen, H. Development and Application of High Throughput Plasma Stability Assay for Drug Discovery. *International Journal of Pharmaceutics* **2005**, *297* (1–2), 110–119. https://doi.org/10.1016/j.ijpharm.2005.03.022.

(32) Hofmans, S.; Berghe, T. V.; Devisscher, L.; Hassannia, B.; Lyssens, S.; Joossens, J.; Van Der Veken, P.; Vandenabeele, P.; Augustyns, K. Novel Ferroptosis Inhibitors with Improved Potency and ADME Properties. *J. Med. Chem.* **2016**,

59 (5), 2041–2053. https://doi.org/10.1021/acs.jmedchem.5b01641.

(33) Van Coillie, S.; Van San, E.; Goetschalckx, I.; Wiernicki, B.; Mukhopadhyay, B.; Tonnus, W.; Choi, S. M.; Roelandt, R.; Dumitrascu, C.; Lamberts, L.; Dams, G.; Weyts, W.; Huysentruyt, J.; Hassannia, B.; Ingold, I.; Lele, S.; Meyer, E.; Berg, M.; Seurinck, R.; Saeys, Y.; Vermeulen, A.; Van Nuijs, A. L. N.; Conrad, M.; Linkermann, A.; Rajapurkar, M.; Vandenabeele, P.; Hoste, E.; Augustyns, K.; Vanden Berghe, T. Targeting Ferroptosis Protects against Experimental (Multi)Organ Dysfunction and Death. *Nat Commun* **2022**, *13* (1), 1046. https://doi.org/10.1038/s41467-022-28718-6.

(34) Homma, T.; Kobayashi, S.; Sato, H.; Fujii, J. Edaravone, a Free Radical Scavenger, Protects against Ferroptotic Cell Death in Vitro. *Experimental Cell Research* **2019**, *384* (1), 111592. https://doi.org/10.1016/j.yexcr.2019.111592.

(35) Mishima, E.; Sato, E.; Ito, J.; Yamada, K.; Suzuki, C.; Oikawa, Y.; Matsuhashi, T.; Kikuchi, K.; Toyohara, T.; Suzuki, T.; Ito, S.; Nakagawa, K.; Abe, T. Drugs Repurposed as Antiferroptosis Agents Suppress Organ Damage, Including AKI, by Functioning as Lipid Peroxyl Radical Scavengers. *JASN* **2020**, *31* (2), 280–296. https://doi.org/10.1681/ASN.2019060570.

(36) Shah, R.; Margison, K.; Pratt, D. A. The Potency of Diarylamine Radical-Trapping Antioxidants as Inhibitors of Ferroptosis Underscores the Role of Autoxidation in the Mechanism of Cell Death. *ACS Chem. Biol.* **2017**, *12* (10), 2538–2545. https://doi.org/10.1021/acschembio.7b00730.

(37) Moosmann, B.; Skutella, T.; Beyer, K.; Behl, C. Protective Activity of Aromatic Amines and Imines against Oxidative Nerve Cell Death. *Biological Chemistry* **2001**, *382* (11). https://doi.org/10.1515/BC.2001.195.

(38) Ogasawara, D.; Konrad, D. B.; Tan, Z. Y.; Carey, K. L.; Luo, J.; Won, S. J.; Li, H.; Carter, T.; DeMeester, K. E.; Njomen, E.; Schreiber, S. L.; Xavier, R. J.; Melillo, B.; Cravatt, B. F. *Chemical Tools to Expand the Ligandable Proteome: Diversity-Oriented Synthesis-Based Photoreactive Stereoprobes*; preprint; Biochemistry, 2024. https://doi.org/10.1101/2024.02.27.582206.

(39) Morstein, J.; Capecchi, A.; Hinnah, K.; Park, B.; Petit-Jacques, J.; Van Lehn, R. C.; Reymond, J.-L.; Trauner, D. Medium-Chain Lipid Conjugation Facilitates Cell-Permeability and Bioactivity. *J. Am. Chem. Soc.* **2022**, *144* (40), 18532–18544. https://doi.org/10.1021/jacs.2c07833.

(40) Haidasz, E. A.; Van Kessel, A. T. M.; Pratt, D. A. A Continuous Visible Light Spectrophotometric Approach To Accurately Determine the Reactivity of Radical-Trapping Antioxidants. *J. Org. Chem.* **2016**, *81* (3), 737–744. https://doi.org/10.1021/acs.joc.5b02183.

(41) Zhao, X.; Huang, W.; Song, D.; Lin, R.; Huang, H.; Huang, J.; Wu, B.; Huang, Y.; Ye, G. The Hydrogen Transfer Reaction between the Substance of Triplet State Thioxanthone and Alkane with Sp3 Hybridization Hydrogen. *J Mol Model* **2020**, *26* (3), 56. https://doi.org/10.1007/s00894-020-4300-4.

(42) Bordwell, F. G.; Harrelson, J. A.; Lynch, T. Y. Homolytic Bond Dissociation Energies for the Cleavage of .Alpha.-Nitrogen-Hydrogen Bonds in Carboxamides, Sulfonamides, and Their Derivatives. The Question of Synergism in Nitrogen-Centered Radicals. *J. Org. Chem.* **1990**, *55* (10), 3337–3341. https://doi.org/10.1021/jo00297a064.

(43) Korotenko, V.; Zipse, H. The Stability of OXYGEN-CENTERED Radicals and Its Response to Hydrogen Bonding Interactions. *J Comput Chem* **2024**, *45* (2), 101–114. https://doi.org/10.1002/jcc.27221.

(44) Bordwell, F. G.; Zhang, X. M.; Cheng, J. P. Bond Dissociation Energies of the Nitrogen-Hydrogen Bonds in Anilines and in the Corresponding Radical Anions. Equilibrium Acidities of Aniline Radical Cations. *J. Org. Chem.* **1993**, *58* (23), 6410–6416. https://doi.org/10.1021/jo00075a041.

(45) Konaka, R.; Kuruma, K.; Terabe, S. Mechanisms of Oxidation of Aniline and Related Compounds in Basic Solution. *J. Am. Chem. Soc.* **1968**, *90* (7), 1801–1806. https://doi.org/10.1021/ja01009a022.

(46) Bordwell, F. G.; Ji, G. Z. Effects of Structural Changes on Acidities and Homolytic Bond Dissociation Energies of the Hydrogen-Nitrogen Bonds in Amidines, Carboxamides, and Thiocarboxamides. *J. Am. Chem. Soc.* **1991**, *113* (22), 8398–8401. https://doi.org/10.1021/ja00022a029.

(47) Scott, K. A.; Cox, P. B.; Njardarson, J. T. Phenols in Pharmaceuticals: Analysis of a Recurring Motif. *J. Med. Chem.* **2022**, *65* (10), 7044–7072. https://doi.org/10.1021/acs.jmedchem.2c00223.

(48) Ford, K. A. Role of Electrostatic Potential in the *in Silico* Prediction of Molecular Bioactivation and Mutagenesis. *Mol. Pharmaceutics* **2013**, *10* (4), 1171–1182. https://doi.org/10.1021/mp3004385.

(49) Murray, M. Mechanisms of Inhibitory and Regulatory Effects of Methylenedioxyphenyl Compounds on Cytochrome P450-Dependent Drug Oxidation. *CDM* **2000**, *1* (1), 67–84. https://doi.org/10.2174/1389200003339270.